Effects of Metal Ions on Photoinduced Electron Transfer in Zinc Porphyrin–Naphthalenediimide Linked Systems

Ken Okamoto,[a] Yukie Mori,[b] Hiroko Yamada,[a] Hiroshi Imahori,*[b] and Shunichi Fukuzumi*[a]

Abstract: Zinc porphyrin–naphthalenediimide (ZnP–NIm) dyads and zinc porphyrin–pyromellitdiimide–naphthalenediimide (ZnP–Im–NIm) triad have been employed to examine the effects of metal ions on photoinduced charge-separation (CS) and charge-recombination (CR) processes in the presence of metal ions (scandium triflate ($Sc(OTf)_3$) or lutetium triflate ($Lu(OTf)_3$), both of which can bind with the radical anion of NIm). Formation of the charge-separated states in the absence and in the presence of Sc^{3+} was confirmed by the appearance of absorption bands due to $ZnP^{\bullet+}$ and $NIm^{\bullet-}$ in the absence of metal ions and of those due to $ZnP^{\bullet+}$ and the $NIm^{\bullet-}/Sc^{3+}$ complex in the presence of Sc^{3+} in the time-resolved transient absorption spectra of dyads and triad. The lifetimes of the charge-separated states in the presence of 1.0×10^{-3} M Sc^{3+} (14 μs for ZnP–NIm, 8.3 μs for ZnP–Im–NIm) are more than ten times longer than those in the absence of metal ions (1.3 μs for ZnP–NIm, 0.33 μs for ZnP–Im–NIm). In contrast, the rate constants of the CS step determined by the fluorescence lifetime measurements are the same, irrespective of the presence or absence of metal ions. This indicates that photoinduced electron transfer from $^1ZnP^*$ to NIm in the presence of Sc^{3+} occurs without involvement of the metal ion to produce $ZnP^{\bullet+}$–$NIm^{\bullet-}$, followed by complexation with Sc^{3+} to afford the $ZnP^{\bullet+}$–$NIm^{\bullet-}/Sc^{3+}$ complex. The one-electron reduction potential (E_{red}) of the NIm moiety in the presence of a metal ion is shifted in a positive direction with increasing metal ion concentration, obeying the Nernst equation, whereas the one-electron oxidation potential of the ZnP moiety remains the same. The driving force dependence of the observed rate constants (k_{ET}) of CS and CR processes in the absence and in the presence of metal ions is well evaluated in terms of the Marcus theory of electron transfer. In the presence of metal ions, the driving force of the CS process is the same as that in the absence of metal ions, whereas the driving force of the CR process decreases with increasing metal ion concentration. The reorganization energy of the CR process also decreases with increasing metal ion concentration, when the CR rate constant becomes independent of the metal ion concentration.

Keywords: electron transfer · Marcus theory · metal ions · porphyrinoids · zinc

Introduction

In the bacterial photosynthetic reaction center, relatively little energy (0.2 eV) is consumed in the rapid initial photoinduced electron transfer step from bacteriochlorophyll dimer [$(BChl)_2$] to bacteriopheophytin (Bphe) on a timescale of 3 ps, whereas the back electron transfer to the ground state occurs on a much slower timescale of ≈0.07 s

[a] K. Okamoto, Dr. H. Yamada, Prof. S. Fukuzumi
Department of Material and Life Science
Graduate School of Engineering
Osaka University, CREST
JAPAN Science and Technology Agency
Suita, Osaka 565-0871 (Japan)
Fax: (+81) 6-6879-7370
E-mail: fukuzumi@ap.chem.eng.osaka-u.ac.jp

[b] Dr. Y. Mori, Prof. H. Imahori
Department of Molecular Engineering
Graduate School of Engineering
Kyoto University, PRESTO
JAPAN Science and Technology Agency
Nishikyo-ku, Kyoto 615-8510 (Japan)
and
Fukui Institute for Fundamental Chemistry, Kyoto University
34-4, Takano-Nishihiraki-cho
Sakyo-ku, Kyoto 606-8103 (Japan)
E-mail: imahori@scl.kyoto-u.ac.jp

Supporting information for this article is available on the WWW under http://www.chemeurj.org/ or from the author. Transient spectra and transient decay at 480 nm of **2** and transient spectra of **1** (S1), derivation of Equation (4) (S2), first-order plots of transient absorption of the charge-separated state of **1** in the presence of Lu^{3+} (S3), that of **2** in the presence of Sc^{3+} (S4), fluorescence decay curves of **1** in the absence and in the presence of Sc^{3+} (S5), and plots of $\ln(k'_{CR}T^{1/2})$ against T^{-1} for the charge recombination processes in **1** in the presence of 2 mM Sc^{3+} (S6).

DOI: 10.1002/chem.200305239

despite the much larger driving force (1.2 eV) in relation to the initial photoinduced electron transfer step.[1] When the free energy change of electron transfer (ΔG^0_{ET}) becomes very negative, the driving force of electron transfer ($-\Delta G^0_{ET}$) can exceed the reorganization energy (λ), the energy required for the structural reorganization of the donor, acceptor, and their solvation spheres upon electron transfer. This region ($-\Delta G^0_{ET} > \lambda$) is generally referred to as the Marcus inverted region, where the electron transfer rate is expected to decrease rather than to increase as the driving force of electron transfer ($-\Delta G^0_{ET}$) increases where the driving force is larger than the reorganization energy of electron transfer ($-\Delta G^0_{ET} > \lambda$).[2,3] In the normal region ($-\Delta G^0_{ET} < \lambda$), the electron transfer rate increases with increasing driving force—namely, increasingly negative ΔG^0_{ET}—but in the Marcus inverted region the opposite is true. In such a case a charge shift reaction from $Bphe^{\bullet-}$ to an electron acceptor quinone (Q_A) occurs much more rapidly, on a timescale of 200 ps, than the back electron transfer, which occurs on a timescale of $\approx$0.07 s. The further charge separation proceeds to achieve a nearly quantitative quantum yield of the final charge-separated state, which has an extremely long lifetime (ca. 1 s).[1] Extensive efforts have been devoted to the development of multi-step electron transfer systems involving the initial photoinduced electron transfer with the use of donor–acceptor (D–A) linked multi-array systems to mimic multistep charge-separation processes in photosynthesis.[2–11] The same strategy as occurs in natural photosynthesis has been chosen to optimize the efficiency of the charge-separation processes: that is, the use of components with small reorganization energies of electron transfer in order to accelerate the forward electron transfer in the Marcus normal region and to decelerate the back electron transfer in the Marcus inverted region. The use of fullerene, which has a small reorganization energy in relation to other electron acceptors such as quinones, has been successful in achieving long-lived charge-separated states.[12–20]

In principle, the totally opposite approach to attaining long-lived charge-separated states—that is, the use of a component with a large reorganization energy, resulting in slow back electron transfer in the Marcus normal region ($-\Delta G^0_{ET} < \lambda$)—is also possible. In such a case, however, the rate of forward electron transfer with a much smaller driving force becomes much smaller than the back electron transfer rate, and so the use of a component with a large organization energy has never been employed in the design of the artificial photosynthetic reaction center. If one could design a system in which the forward electron transfer had a small reorganization energy whereas the reorganization energy of the back electron transfer were much larger than that of the forward electron transfer in the Marcus normal region, long-lived charge-separated states would be attained efficiently. In the Marcus normal region, the smaller the driving force, the smaller is the electron transfer rate. Thus, a decrease in the driving force of back electron transfer is essential to attain the long-lived charge-separated states in the Marcus normal region.

It has been shown that the driving force of electron transfer can be finely controlled by complexation of radical anions, produced in the electron transfer, with metal ions acting as Lewis acids, in a variety of intermolecular and intramolecular electron transfer systems.[21–25] Quantitative measurements to determine the Lewis acidity of a variety of metal ions have now been established in relation to the promoting effects of metal ions on the electron transfer reactions.[26]

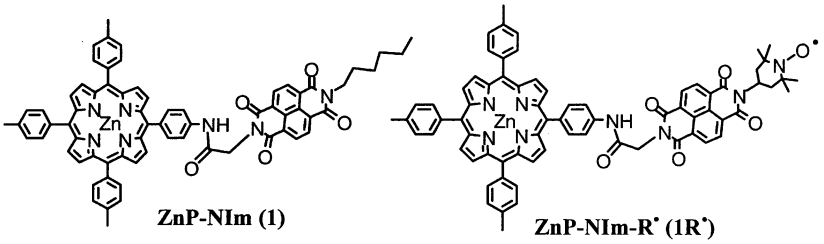

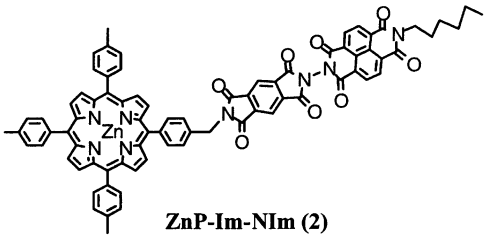

Here we report the effects of metal ions on photoinduced electron transfer in porphyrin-containing donor–acceptor ensembles, zinc porphyrin–naphthalenediimide (ZnP–NIm) dyads and zinc porphyrin–pyromellitdiimide–naphthalenediimide (ZnP–Im–NIm) triad.[27] Here, naphthalenediimide, employed as an electron acceptor moiety containing a carbonyl oxygen, plays an important role in binding with metal ions in the radical anion state ($NIm^{\bullet-}$). The driving force of back electron transfer from the $NIm^{\bullet-}$ moiety to the $ZnP^{\bullet+}$ can be controlled by addition of metal ions, which bind with $NIm^{\bullet-}$. The strong binding of metal ions with $NIm^{\bullet-}$ results in a decrease in the driving force of back electron transfer and an increase in the reorganization energy of electron transfer. In contrast to that of the back electron-transfer process, the driving force of forward photoinduced electron transfer remains the same irrespective of the absence or presence of metal ions, since the photoinduced charge separation process occurs without involvement of metal ions, which bind with the $NIm^{\bullet-}$ moiety only after the electron transfer. This study thus provides a new strategy by which to attain long-lived charge-separated states in the Marcus normal region with a large reorganization energy.

Results and Discussion

Photoinduced intramolecular electron transfer: Time-resolved transient absorption spectra of ZnP–NIm (**1**), ZnP–Im–NIm (**2**), and ZnP–NIm–R$^{\bullet}$ (**1R**$^{\bullet}$) in benzonitrile (PhCN) were measured by nanosecond laser photolysis. A transient absorption spectrum observed at 0.1 μs after the laser pulse excitation of a PhCN solution of **1** is shown in Figure 1a. The transient absorption bands at 479, 531, 583, 620, 685 (sh), and 763 nm are attributable to NIm$^{\bullet-}$ by comparison with those of NIm$^{\bullet-}$ produced independently by the one-electron reduction of **1** with tetramethylsemiquinone radical anion (Scheme 1, Figure 1b).[28] The absorption band due to ZnP$^{\bullet+}$ is also observed at 410 nm (Figure 1a).[29]

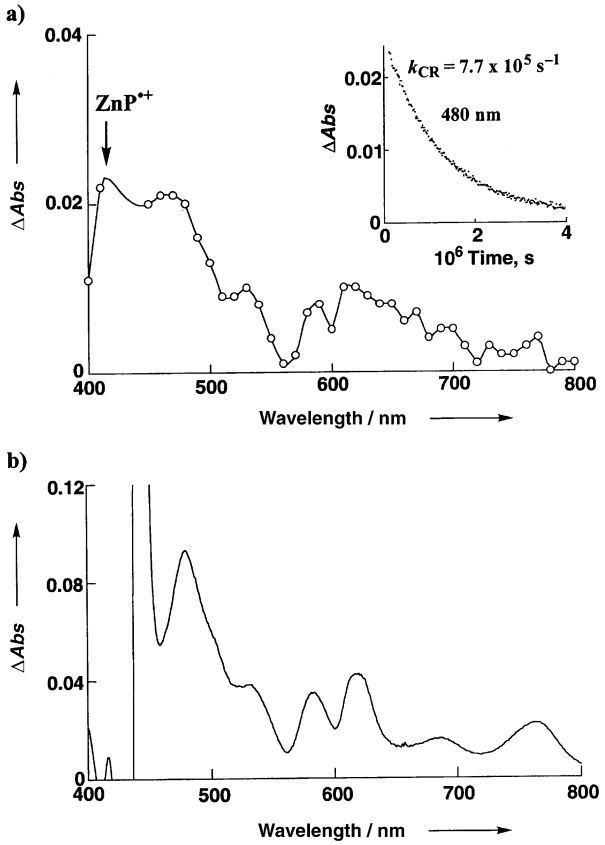

Figure 1. a) Time-resolved absorption spectrum observed at 0.1 μs after laser pulse excitation (431 nm) of a deaerated PhCN solution of **1** (1.0×10^{-5} M) at 298 K. Inset: Time profile of absorbance at 480 nm. b) The difference spectrum of the radical anion of **1** (1.0×10^{-5} M), in which the spectrum due to **1** (1.0×10^{-5} M) is subtracted. The radical anion of **1** was generated by the one-electron reduction of **1** with tetramethylsemiquinone radical anion in deaerated PhCN at 298 K.

Each absorption band decays at the same rate, obeying first-order kinetics (inset of Figure 1a). From the first-order plot it is possible to obtain the rate constant (k_{CR}) of the charge-recombination (CR) process in the charge-separated state—ZnP$^{\bullet+}$–NIm$^{\bullet-}$—as 7.7×10^5 s^{-1} (lifetime of the charge-separated state: τ_{CS} = 1.3 μs). Similarly, the k_{CR} rate constants can be determined from the decay of the charge-separated states of **2** (see Supporting Information S1) and **1R**$^{\bullet}$, and the k_{CR} values are listed in Table 1.

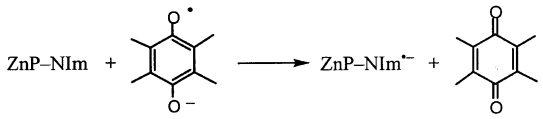

Scheme 1. Independent production of **1**.

The addition of Sc(OTf)$_3$ to a PhCN solution of **1** results in a change in the transient absorption spectrum in relation to that in the absence of Sc(OTf)$_3$. Figure 2a shows transient absorption spectra observed at 0.1 μs and 1 μs after the laser pulse excitation of a PhCN solution of **1** in the presence of Sc(OTf)$_3$ (2.0×10^{-3} M). At 0.1 μs, besides the absorption bands due to ZnP$^{\bullet+}$ and NIm$^{\bullet-}$, a new absorption band, not seen in the absence of Sc(OTf)$_3$, is observed at 650 nm.[30] At 1 μs, the absorption bands due to NIm$^{\bullet-}$ are changed to those of the new bands, which can be assigned to the Sc^{3+} complex with NIm$^{\bullet-}$ by comparison with the transient absorption bands observed by photoexcitation of a PhCN solution of 1-benzyl-1,4-dihydronicotinamide dimer [(BNA)$_2$] and NIm-ref in Figure 2b.[31] It has been well established that photoinduced electron transfer from (BNA)$_2$ to electron acceptors in the presence of metal ions affords the metal ion complexes with radical anions.[32] Thus, photoinduced electron transfer from (BNA)$_2$ to NIm-ref in the presence of Sc(OTf)$_3$ affords the (NIm-ref)$^{\bullet-}$/Sc^{3+} complex (Scheme 2). The results in Figure 2a therefore indicate that photoinduced electron transfer from the porphyrin singlet excited state (^{1}ZnP*) to NIm in the presence of Sc(OTf)$_3$ initially produces the charge-separated state, ZnP$^{\bullet+}$–NIm$^{\bullet-}$, and that the NIm$^{\bullet-}$ moiety then forms the complex with Sc(OTf)$_3$ to give the ZnP$^{\bullet+}$–NIm$^{\bullet-}$/Sc^{3+} complex.

The CR process in the ZnP$^{\bullet+}$–NIm$^{\bullet-}$/Sc^{3+} complex in the presence of Sc(OTf)$_3$ is followed by the decay of absorbance at 480 nm and is compared in Figure 3 with the CR process in ZnP$^{\bullet+}$–NIm$^{\bullet-}$ in the absence of metal ions. The decay of

Table 1. Driving forces ($-\Delta G_{ET(CR)}$) and electron transfer rate constants (k_{CR}) of CR in **1**, **2**, and **1R**$^{\bullet}$ in deaerated PhCN at 298 K.

		1			**2**			**1R**$^{\bullet}$		
M^{n+}	$[M^{n+}]$ / M	no.	k_{CR} / s^{-1}	$-\Delta G_{ET(CR)}$[a] / eV	no.	k_{CR} / s^{-1}	$-\Delta G_{ET(CR)}$[a] / eV	no.	k_{CR} / s^{-1}	$-\Delta G_{ET(CR)}$[a] / eV
Sc^{3+}	0	1	7.7×10^5	1.33	10	3.0×10^6	1.22	19	6.2×10^5	1.32
	2.0×10^{-4}	2	6.9×10^4	0.84	11	1.2×10^5	0.98	20	2.1×10^5	1.20
	1.0×10^{-3}	3	6.9×10^4	0.80	12	1.2×10^5	0.94	21	2.1×10^5	1.16
	2.0×10^{-3}	4	6.9×10^4	0.79	13	1.2×10^5	0.92	22	2.1×10^5	1.15
	4.0×10^{-3}	5	6.9×10^4	0.77	14	1.2×10^5	0.90	23	2.1×10^5	1.13
Lu^{3+}	2.0×10^{-4}	6	7.6×10^4	0.98	15	4.0×10^5	1.13	–	–	
	1.0×10^{-3}	7	7.6×10^4	0.94	16	4.0×10^5	1.09	–	–	
	2.0×10^{-3}	8	7.6×10^4	0.92	17	4.0×10^5	1.07	–	–	
	4.0×10^{-3}	9	7.6×10^4	0.90	18	4.0×10^5	1.05	–	–	

[a] Determined from Equation (7).

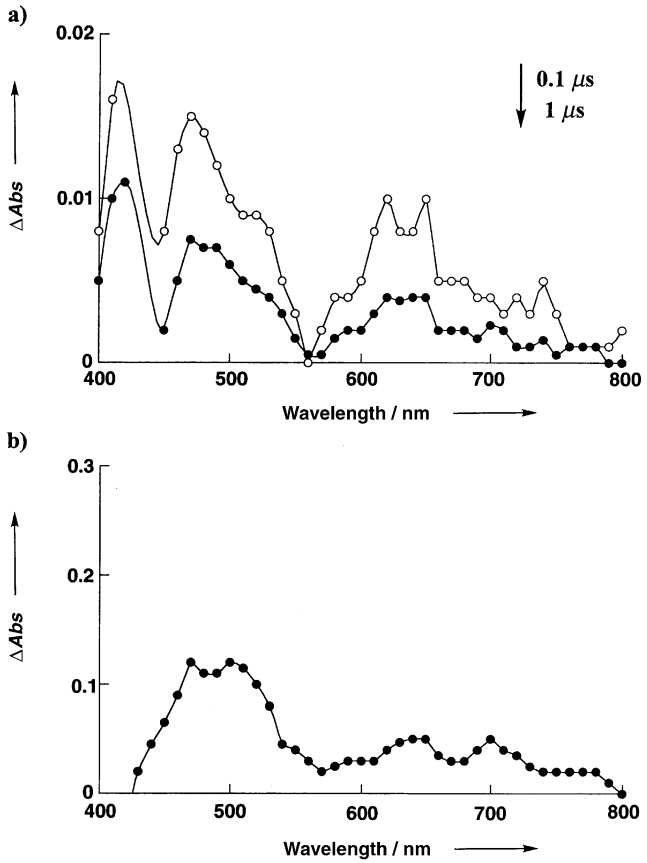

Figure 2. a) Time-resolved absorption spectra observed at 0.1 μs (○) and 1 μs (●) after laser pulse excitation (431 nm) of a deaerated PhCN solution of **1** (1.0×10^{-5} M) in the presence of $Sc(OTf)_3$ (2.0×10^{-3} M) at 298 K. b) Time-resolved absorption spectrum of the $(NIm\text{-}ref)^{\bullet-}/Sc^{3+}$ complex produced by the photoinduced electron transfer from $(BNA)_2$ (5.0×10^{-2} M) to NIm-ref (1.0×10^{-4} M) in the presence of 2.0×10^{-2} M Sc^{3+} in deaerated PhCN at 10 μs after laser pulse excitation (355 nm) at 298 K.

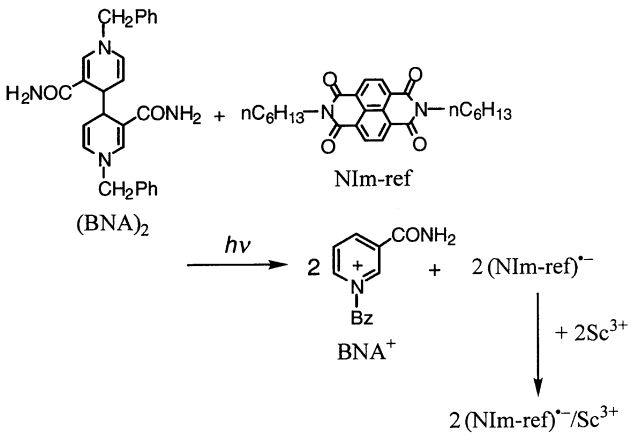

Scheme 2. Photoinduced electron transfer from $(BNA)_2$ to NIm-ref in the presence of $Sc(OTf)_3$, affording the $(NIm\text{-}ref)^{\bullet-}/Sc^{3+}$ complex.

$ZnP^{\bullet+}$–$NIm^{\bullet-}$ in the absence of $Sc(OTf)_3$ obeys first-order kinetics [Eq. (1)]. In the presence of $Sc(OTf)_3$, however, the decay consists of two components (closed circles in Figure 3). The larger the concentration of $Sc(OTf)_3$, the larger is the contribution of the slow component, which has the same lifetime irrespective of any difference in $Sc(OTf)_3$ concentration. The initial fast component thus corresponds to the complexation process of Sc^{3+} with the $NIm^{\bullet-}$ moiety in $ZnP^{\bullet+}$–$NIm^{\bullet-}$ to produce the $ZnP^{\bullet+}$–$NIm^{\bullet-}/Sc^{3+}$ complex [Eq. (2)], which decays to the ground state with a much slower rate constant (k'_{CR}) [Eq. (3)].

$$ZnP^{\bullet+} - NIm^{\bullet-} \xrightarrow{k_{CR}} ZnP - NIm \quad (1)$$

$$ZnP^{\bullet+} - NIm^{\bullet-} + Sc^{3+} \xrightarrow{k_1} ZnP^{\bullet+} - NIm^{\bullet-}/Sc^{3+} \quad (2)$$

$$ZnP^{\bullet+} - NIm^{\bullet-}/Sc^{3+} \xrightarrow{k'_{CR}} ZnP - NIm + Sc^{3+} \quad (3)$$

According to Equations (1)–(3), the sum of the concentrations of $ZnP^{\bullet+}$–$NIm^{\bullet-}$ and the $ZnP^{\bullet+}$–$NIm^{\bullet-}/Sc^{3+}$ complex is given by Equation (4) (for the derivation see Supporting Information). Equation (4) predicts the two-exponential decay. The k_{CR} value in the absence of $Sc(OTf)_3$ is determined as $7.7\times10^5\ s^{-1}$ from the slope of the linear first-order plot in Figure 3 (open circles). The k'_{CR} rate constant of the $ZnP^{\bullet+}$–$NIm^{\bullet-}/Sc^{3+}$

$$[ZnP^{\bullet+} - NIm^{\bullet-}] + [ZnP^{\bullet+} - NIm^{\bullet-}/Sc^{3+}] = \frac{[ZnP^{\bullet+} - NIm^{\bullet-}]_0}{k_{CR} + k_1[Sc^{3+}] - k'_{CR}} [(k_{CR} - k'_{CR}) \exp\{-(k_{CR} + k_1[Sc^{3+}])t\} + k_1[Sc^{3+}] \exp(-k'_{CR}t)] \quad (4)$$

complex is determined as $6.9\times10^4\ s^{-1}$ from the constant slope after the completion of the complexation process of Sc^{3+} with $NIm^{\bullet-}$ (Figure 3).[33] From the initial slope in Figure 3 it is possible to estimate the k_1 value as about $1\times10^8\ M^{-1}\ s^{-1}$. Thus, the rate of the complexation process of Sc^{3+} with the $NIm^{\bullet-}$ moiety in $ZnP^{\bullet+}$–$NIm^{\bullet-}$ is much faster than the CR rate. The k'_{CR} values in the presence of $Sc(OTf)_3$ become significantly smaller in relation to the k_{CR} value in the absence of $Sc(OTf)_3$ ($7.7\times10^5\ s^{-1}$), which indicates that the lifetime of the charge-separated state becomes

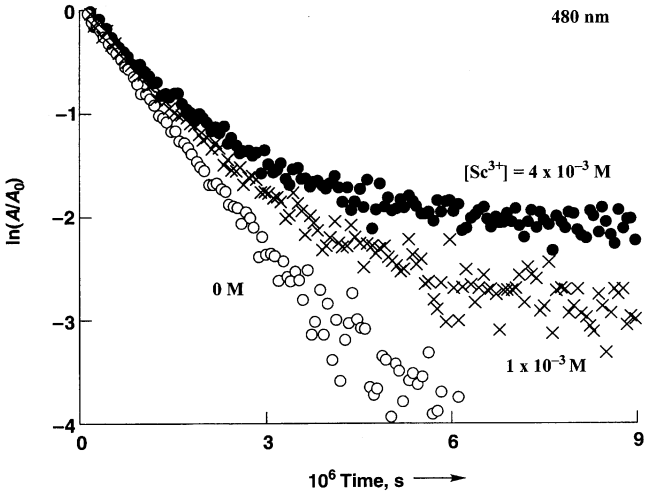

Figure 3. First-order plots of the observed absorption change at 480 nm after laser pulse excitation (431 nm) of a deaerated PhCN solution of **1** (1.0×10^{-5} M) in the absence and in the presence of $Sc(OTf)_3$ at 298 K; $[Sc^{3+}] = 0$ (○), 1.0×10^{-3} M (×), and 4.0×10^{-3} M (●).

much longer through the complexation with $Sc(OTf)_3$. Similarly, the k'_{CR} values of other metal ion complexes of the charge-separated states of **1** (see Figure S3 in the Supporting Information), **2** (see Figure S4 in the Supporting Information), and **1R**$^{\bullet}$ in the presence of various concentrations of $Sc(OTf)_3$ and $Lu(OTf)_3$ are determined as listed in Table 1.[34,35]

The rate constants of photoinduced electron transfer from $^1ZnP^*$ to NIm to give the charge-separated states (k_{CS}) were determined by fluorescence lifetime measurements in PhCN. The k_{CS} value of **1** in PhCN is determined from the difference between τ^{-1} and $\tau_{(ZnP\text{-}ref)}{}^{-1}$ as $3.4\times10^9\ s^{-1}$. Similarly, the k_{CS} values of **2** and **1R**$^{\bullet}$ are determined as listed in Table 2.[36]

The k_{CS} values were also determined in the presence of various concentrations of $Sc(OTf)_3$ and $Lu(OTf)_3$, and the results are listed in Table 2. In contrast with the k_{CR} values, the k_{CS} values are the same irrespective of the presence or absence of $Sc(OTf)_3$ (see Figure S5 in the Supporting Information). This is consistent with the results in Figure 2, where the photoinduced electron transfer from $^1ZnP^*$ to NIm in the presence of $Sc(OTf)_3$ affords the charge-separated state ($ZnP^{\bullet+}$–$NIm^{\bullet-}$) and the complexation with $Sc(OTf)_3$ then occurs to produce the $ZnP^{\bullet+}$–$NIm^{\bullet-}/Sc^{3+}$ complex. Thus, the rate of the initial photoinduced electron transfer is not affected by the presence of metal ions.

Driving force of electron-transfer processes in the presence of metal ion salts: To determine the driving force of electron transfer, the one-electron redox potentials of **1**, **2**, and **1R**$^{\bullet}$ in the absence and in the presence of metal ions were determined by cyclic voltammetry in PhCN. Figure 4 shows cyclic voltammograms of **1** in the absence and in the presence of $Sc(OTf)_3$. The one-electron reduction potential at −0.57 V for the NIm/$NIm^{\bullet-}$ couple is shifted in a positive direction by 0.55 V in the presence of 3.0×10^{-3} M $Sc(OTf)_3$, whereas the one-electron oxidation potential of ZnP at 0.76 V remains the same irrespective of the absence or presence of $Sc(OTf)_3$. Similar positive shifts of the one-electron reduction potential of NIm (E_{red}) are observed in the presence of $Lu(OTf)_3$.

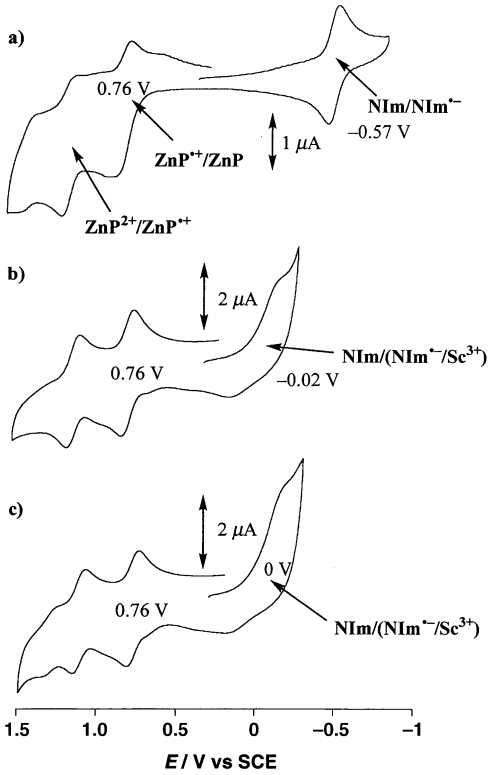

Figure 4. Cyclic voltammograms of **1** (5.0×10^{-4} M): a) in the absence of Sc^{3+}, b) in the presence of 3.0×10^{-3} M Sc^{3+}, and c) in the presence of 5.0×10^{-3} M Sc^{3+} in deaerated PhCN containing $TBAPF_6$ (0.10 M) at 298 K.

Table 2. Driving forces ($-\Delta G_{ET(CS)}$) and electron transfer rate constants (k_{CS}) of CS in **1**, **2**, and **1R**$^{\bullet}$ in deaerated PhCN at 298 K.

No.	Compound	$[M^{n+}]$ (M)	Solvent	$-\Delta G_{ET(CS)}$ (eV)	k_{CS} (s^{-1})
1	**1**	0	THF	0.57	7.7×10^{9}[b]
2		0	PrCN	0.79	6.2×10^{9}[b]
3		0	MeCN	0.81	4.1×10^{9}[b]
4		0	PhCN	0.81	3.4×10^{9}[c]
5	**1**+Sc^{3+}	2.0×10^{-3}	PhCN	0.27[a]	3.4×10^{9}[c]
6		4.0×10^{-3}	PhCN	0.25[a]	3.4×10^{9}[c]
7	**1**+Lu^{3+}	4.0×10^{-3}	PhCN	0.38[a]	3.4×10^{9}[c]
8	**2**	0	THF	0.64	6.1×10^{9}[b]
9		0	PrCN	0.88	6.2×10^{9}[b]
10		0	MeCN	0.90	4.6×10^{9}[b]
11		0	PhCN	0.92	3.1×10^{8}[c]
12	**2**+Sc^{3+}	2.0×10^{-3}	PhCN	0.62[a]	3.1×10^{8}[c]
13		4.0×10^{-3}	PhCN	0.60[a]	3.1×10^{8}[c]
14	**2**+Lu^{3+}	4.0×10^{-3}	PhCN	0.75[a]	3.1×10^{8}[c]
15	**1R**$^{\bullet}$	0	PhCN	0.80	6.9×10^{9}[c]
16	**1R**$^{\bullet}$+Sc^{3+}	4.0×10^{-3}	PhCN	0.61[a]	6.9×10^{9}[c]

[a] Determined from Equation (9). [b] Taken from ref. [27]. [c] This work; $k_{CS} = \tau_{(\mathbf{1},\mathbf{2},\mathbf{1R})}{}^{-1} - \tau_{(ZnP)}{}^{-1}$

The positive shift of E_{red} in the presence of metal ions is attributable to the binding of metal ions with $NIm^{\bullet-}$ [Eq. (5)] as indicated in Figure 4. The neutral species of NIm cannot bind with Sc^{3+}, since there was no carbonyl peak shift [δ = 162 ppm ($CDCl_3/CD_3CN$ 1:1)] in ^{13}C NMR measurements irrespective of the presence of Sc^{3+}. In such a case, E_{red} is given as a function of concentration of metal ions (M^{n+}), according to the Nernst equation [Eq. (6)],[37] where E^0_{red} is the one-electron reduction potential in the absence of metal ions, K_{red} is the formation constant of the ZnP–$NIm^{\bullet-}/M^{n+}$ complex, K_{ox} is the formation constant of the ZnP–NIm/M^{n+} complex, R is the gas constant, T is the absolute temperature, and F is the Faraday constant. Since $K_{red}[M^{n+}] \gg 1$, and $K_{ox}[M^{n+}] \ll 1$, Equation (6) can be reformulated as Equation (7), where ΔE_{red} is the potential shift in the presence of M^{n+} from the value in its absence.

$$ZnP - NIm^{\bullet-} + M^{n+} \underset{K_{red}}{\rightleftharpoons} ZnP - NIm^{\bullet-}/M^{n+} \quad (5)$$

$$E_{red} = E^0_{red} + (RT/F)\ln\left\{\frac{(1+K_{red}[M^{n+}])}{(1+K_{ox}[M^{n+}])}\right\} \quad (6)$$

$$\Delta E_{red} = (RT/F)\ln K_{red}[M^{n+}] \quad (7)$$

Plots of ΔE_{red} against $\log[M^{n+}]$ ($M^{n+} = Sc^{3+}$ and Lu^{3+}) are shown in Figure 5. The slope of each plot is determined

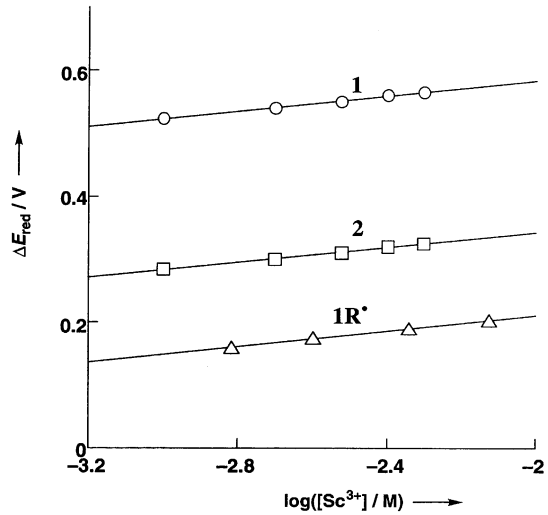

Figure 5. Nernst plots of ΔE_{red} against $\log[Sc^{3+}]$ for **1** (○), **2** (□), and **1R**• (△). The slope of the line is 0.059.

as 0.059, which agrees with the slope ($2.3RT/F$ at 298 K) expected from the Nernst equation [Eq. (7)]. The intercepts of linear plots in Figure 5 thus afford the binding constants of **1** ($K_{red}(Sc^{3+}) = 8.7\times10^{11}\,M^{-1}$, $K_{red}(Lu^{3+}) = 4.3\times10^{9}\,M^{-1}$), **2** ($K_{red}(Sc^{3+}) = 6.5\times10^{7}\,M^{-1}$, $K_{red}(Lu^{3+}) = 1.2\times10^{5}\,M^{-1}$), and **1R**• ($K_{red}(Sc^{3+}) = 4.7\times10^{5}\,M^{-1}$). These K_{red} values are much smaller than the reported values of $Q^{\bullet-}/Sc^{3+}$ and $NQ^{\bullet-}/Sc^{3+}$.[25]

The driving force of the CS process in the absence of M^{n+} ($-\Delta G^0_{ET(CS)}$ in eV) and that in the presence of M^{n+} ($-\Delta G_{ET(CS)}$ in eV) are given by Equation (8) and Equation (9), respectively,

$$-\Delta G^0_{ET(CS)} = -e[E^0(ZnP^{\bullet+}/{}^1ZnP^*) - E^0(NIm/NIm^{\bullet-})] \quad (8)$$

$$-\Delta G_{ET(CS)} = -\Delta G^0_{ET(CS)} + k_B T\ln(K_{red}[M^{n+}]) \quad (9)$$

where e is the elementary charge and k_B is the Boltzmann constant. On the other hand, the driving force of the CR process in the absence of M^{n+} ($-\Delta G^0_{ET(CR)}$) and that in the presence of M^{n+} ($-\Delta G_{ET(CR)}$) are given by Equation (10) and Equation (11), respectively, where $\Delta E({}^1ZnP^*/ZnP)$ is the singlet excitation energy of ZnP.

$$-\Delta G^0_{ET(CR)} = \Delta G^0_{ET(CS)} + \Delta E({}^1ZnP^*/ZnP) \quad (10)$$

$$-\Delta G_{ET(CR)} = -\Delta G^0_{ET(CR)} - k_B T\ln(K_{red}[M^{n+}]) \quad (11)$$

It is important to note here that the driving force of the CS process increases with increasing metal ion concentration $[M^{n+}]$ [Eq. (9)], but that the driving force of the CR process decreases with increasing $[M^{n+}]$ [Eq. (11)].

The energy diagram of photoinduced electron transfer and the back electron transfer of **1** is shown in Figure 6. The

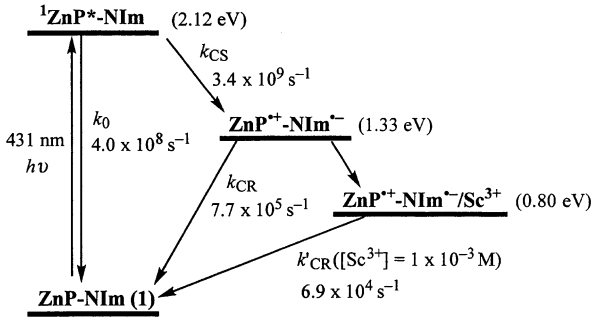

Figure 6. Energy diagram of photoinduced electron transfer and back electron transfer of **1**.

photoexcitation of **1** results in the formation of the singlet excited state $^1ZnP^*$–NIm (2.12 eV), in which electron transfer from $^1ZnP^*$ to NIm occurs to give the charge-separated state ($ZnP^{\bullet+}$–$NIm^{\bullet-}$) with $k_{CS} = 3.4\times10^9\,s^{-1}$ in competition with the decay to the ground state with $k_0 = 4.0\times10^8\,s^{-1}$. Intersystem crossing (ISC) from $^1ZnP^*$ also occurs to give the triplet excited state $^3ZnP^*$, but electron transfer from $^3ZnP^*$ to NIm occurs to produce the charge-separated state as well. The back electron transfer from $NIm^{\bullet-}$ to $ZnP^{\bullet+}$ (CR) occurs with $k_{CR} = 7.7\times10^5\,s^{-1}$.

In the presence of M^{n+}, the CS process takes place mainly from $^1ZnP^*$–NIm rather than $^1ZnP^*$–NIm/M^{n+} complex due to very weak binding of M^{n+} with neutral species of NIm. Furthermore, the observed spectral change shown in Figure 2a indicates that the CS process is not coupled with the binding of Sc^{3+} with $NIm^{\bullet-}$, which occurs after the CS process. This corresponds to the case in which electron transfer occurs first, followed by ion transfer in the effects of electrolytes for ion pairing on the rates of electron transfer reactions, reported by Marcus.[38] In such a case, the k_{CS} values in the presence of M^{n+} are determined by the $-\Delta G^0_{ET(CS)}$ values in the absence of M^{n+} [Eq. (8)] rather than by the $-\Delta G_{ET(CS)}$ values in the presence of M^{n+} [Eq. (9)], although the $-\Delta G_{ET(CS)}$ values increase with increasing $[M^{n+}]$ [Eq. (9)]. In contrast, the k'_{CR} values in the presence of M^{n+} should be determined by the $-\Delta G_{ET(CR)}$ values in the presence of M^{n+}, since the CR process occurs mainly from the $ZnP^{\bullet+}$–$NIm^{\bullet-}$/M^{n+} complex rather than from $ZnP^{\bullet+}$–$NIm^{\bullet-}$, as shown in Figure 2a in the case of the $ZnP^{\bullet+}$–$NIm^{\bullet-}$/Sc^{3+} complex. The back electron transfer from $NIm^{\bullet-}$ to $ZnP^{\bullet+}$ (CR) in the presence of $1.0\times10^{-3}\,M$ Sc^{3+} occurs with $k'_{CR} = 6.9\times10^4\,s^{-1}$.

Driving force dependence of rate constants of CS and CR processes in the absence and in the presence of metal ions: The driving force dependence of the rate constants of electron transfer ($\log k_{ET}$) including both the CS and CR processes in the absence of M^{n+} is shown in Figure 7 (part a), in which the k_{ET} and $-\Delta G^0_{ET}$ values are taken from Table 1 and

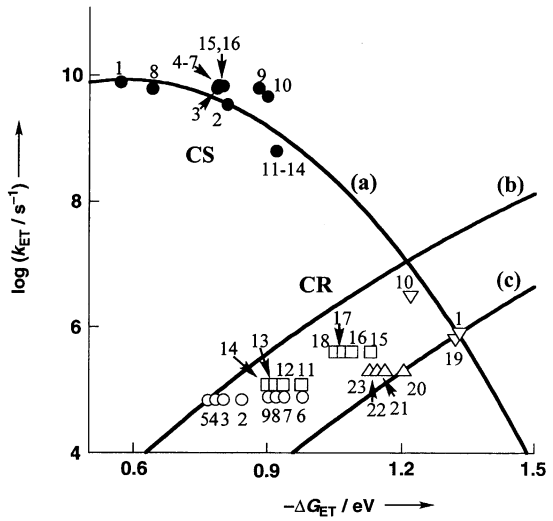

Figure 7. Driving force ($-\Delta G_{ET}$) dependence of intramolecular electron transfer rate constants for CS (●) and CR (▽) in the absence of M^{n+}, and for CR (**1** (○), **2** (□) and **1R**$^{\bullet}$ (△)) in the presence of M^{n+} in deaerated PhCN at 298 K. Numbers refer to compounds in Table 1 (CR) and Table 2 (CS). The solid lines [(a), (b), and (c)] represent the fits to Equation (12) with: a) $\lambda = 0.58$ eV, $V = 5.0\,cm^{-1}$, b) $\lambda = 2.43$ eV, $V = 5.0\,cm^{-1}$, and c) $\lambda = 2.93$ eV, $V = 5.0\,cm^{-1}$.

Table 2. The log k_{CS} value in the absence of metal ions decreases rather than increases with increasing driving force. The k_{CR} values are much smaller than the k_{CS} values despite the driving force of the CR process being much larger than that of the CS process. This indicates that the CS process is already in the Marcus inverted region and that the CR process is deeply in the inverted region.[2–3] Such driving force dependence of log k_{ET} in Figure 7 (part a) can be analyzed in terms of the Marcus equation for non-adiabatic intramolecular electron transfer [Eq. (12) and Eq. (13)], where λ is the reorganization energy of electron transfer, V is the coupling matrix element, and h is the Planck constant.[2]

$$k_{ET} = (4\pi^3/h^2\lambda k_B T)^{1/2} V^2 \exp(-\Delta G_{ET}^{\pm}/k_B T) \quad (12)$$

$$\Delta G_{ET}^{\pm} = (\lambda/4)(1 + \Delta G_{ET}/\lambda)^2 \quad (13)$$

The reasonable fit to a single Marcus curve of all the data in the absence of M^{n+} in Table 1 affords the values of $\lambda = 0.58$ eV and $V = 5.0\,cm^{-1}$ (Figure 7a), which should be regarded as average values of the investigated compounds, since the λ and V values vary slightly depending on the different geometry or solvation. It is more important to point out that the k_{CS} values in the presence of M^{n+} are also included in the single correlation in the absence of M^{n+} using the driving force in the absence of M^{n+}. This indicates that the change in the driving force of the CS process in the presence of M^{n+} does not affect the CS rate, because the binding of M^{n+} with $NIm^{\bullet-}$, which causes the change in the driving force, occurs after the photoinduced electron transfer.

In contrast to the CS process in the presence of M^{n+}, the k'_{CR} values in the presence of M^{n+} become much smaller than those in the absence of M^{n+}, but the decreased k'_{CR} values are fairly constant irrespective of the difference in the driving force, as shown in Figure 7. The solid lines in Figure 7 (part b and part c) represent the lines calculated by use of the same V value for the line in the absence of M^{n+} (part a) but also of two different λ values: $\lambda = 2.43$ eV and 2.93 eV, respectively.[32c] Such large λ values are required to fit the data in the presence of M^{n+} to Equation (12). According to Equation (12) and Equation (13), k'_{CR} should exhibit a significant temperature dependence, since the $\Delta G_{ET}^{\pm}$ value of the CR process of the $ZnP^{\bullet+}$–$NIm^{\bullet-}/Sc^{3+}$ complex is obtained as 0.29 eV from the λ and the $\Delta G_{ET(CR)}$ values in the case of 2.0×10^{-3} M Sc^{3+}. The temperature dependence of the k'_{CR} was also determined and a plot of $\ln(k'_{CR}T^{1/2})$ against T^{-1} gave a linear correlation, as expected from Equation (12) (S6). From the linear slope it is possible to determine the $\Delta H_{ET}^{\pm}$ value as 0.21 eV, which is smaller than the $\Delta G_{ET}^{\pm}$ value because $\Delta G_{ET}^{\pm} = \Delta H_{ET}^{\pm} - T\Delta S_{ET}^{\pm}$ in which the activation entropy ($\Delta S_{ET}^{\pm}$) is negative in non-adiabatic electron transfer.

The driving force dependence of k'_{CR} in the presence of M^{n+} in Figure 7 (part b and part c) indicates that the λ value is not constant but varies with the driving force. Such a change in the λ value with $[M^{n+}]$ can be evaluated in the context of the Marcus theory of electron transfer as follows. The λ value consists of λ_D for the electron self-exchange between D and $D^{\bullet+}$ and λ_A for that between A and $A^{\bullet-}$ [Eq. (14)].

$$\lambda = (\lambda_D + \lambda_A)/2 \quad (14)$$

Since M^{n+} is involved only for the acceptor part (NIm), the dependence of λ_A on $[M^{n+}]$ should be considered. The electron self-exchange between ZnP–NIm and the ZnP–$NIm^{\bullet-}/M^{n+}$ complex occurs through the formation of the ZnP–NIm/M^{n+} complex as shown in Scheme 3.

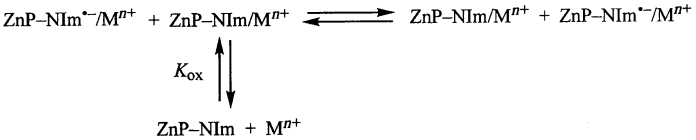

Scheme 3. Electron self-exchange between ZnP–NIm and the ZnP–$NIm^{\bullet-}/M^{n+}$ complex.

According to Scheme 3, the electron self-exchange rate constant (k_{ex}) is given by Equation (15), where Z is the frequency factor for an intermolecular reaction, $\lambda^0{}_A$ is the reorganization energy for the electron self-exchange between the ZnP–NIm/M^{n+} and ZnP–$NIm^{\bullet-}/M^{n+}$ complexes.

$$k_{ex} = ZK_{ox}[M^{n+}]\exp(-\lambda_A^0/4k_B T) \quad (15)$$

The reorganization energy between ZnP–NIm and the ZnP–$NIm^{\bullet-}/M^{n+}$ complex (λ_A) is therefore given by Equation (16), from comparison of Equation (15) with $k_{ex} = Z\exp(-\lambda_A/4k_B T)$. From Equation (15), the reorganization energy λ is given by Equation (17), where $\lambda^0 = (\lambda_D + \lambda_A^0)/2$. Equation (17) indicates that the λ value decreases with increasing $[M^{n+}]$ as observed in Figure 7.

$$\lambda_A = \lambda_A^0 - 4k_B T \ln (K_{ox}[M^{n+}]) \quad (16)$$

$$\lambda = \lambda^0 - 2k_B T \ln (K_{ox}[M^{n+}]) \quad (17)$$

Since $\lambda \gg -\Delta G_{ET(CR)}$ in Figure 7, the Marcus free parabolic energy relationship [Eq. (13)] is simplified to Equation (18) under these experimental conditions for the CR process. The differential of Equation (18) with respect to $\Delta G_{ET(CR)}$ is given by Equation (19). The zero value of $\partial(\Delta G^{\neq}_{ET(CR)})/\partial(\Delta G_{ET(CR)})$ means that the k'_{CR} value should be constant irrespective of the difference in the driving force at various concentrations of M^{n+}. Such a constant driving force dependence of k'_{CR} with variation of $[M^{n+}]$ is indeed observed experimentally, as shown in Figure 7.

$$\Delta G^{\neq}_{ET(CR)} = (\lambda/4) + (\Delta G_{ET(CR)}/2) \quad (18)$$

$$\partial(\Delta G^{\neq}_{ET(CR)})/\partial(\Delta G_{ET(CR)}) = (1/4)\partial(\lambda)/\partial(\Delta G_{ET(CR)}) + 0.5 = 0 \quad (19)$$

The driving force dependence of k'_{CR} is derived from Equation (12), Equation (17), and Equation (18) as Equation (20) and Equation (21). Figure 8 shows plots of $-k_B T \ln (k'_{CR}/[M^{n+}]^{1/2})$ against $\Delta G_{ET(CR)}$ including all data in Table 1.

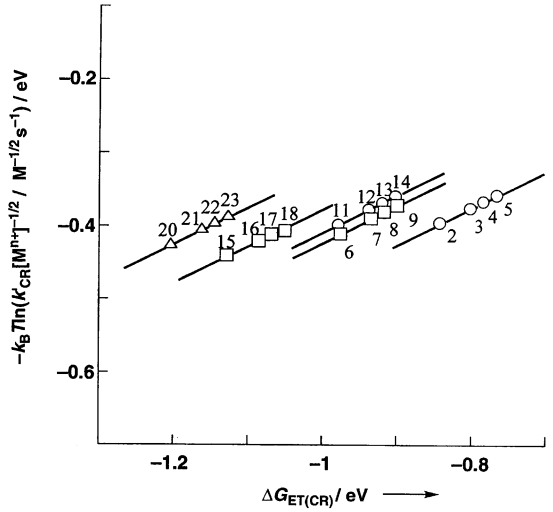

Figure 8. Plots of $-k_B T \ln (k'_{CR}[M^{n+}]^{-1/2})$ against $\Delta G_{ET(CR)}$ for the CR processes in **1** (○), **2** (□) and **1R**• (△) in the presence of M^{n+} in PhCN. Numbers refer to compounds in Table 2. The slope of each plot is 0.50.

$$-k_B T \ln (k'_{CR}/[M^{n+}]^{1/2}) = C + (\Delta G_{ET(CR)}/2) \quad (20)$$

$$C = (\lambda^0/4) - k_B T \ln [V^2 (4\pi^3 K_{ox}/h^2 \lambda k_B T)^{1/2}] \quad (21)$$

Each of the plots gave a straight line, indicating that C is nearly independent of concentration of M^{n+} but depends on the type of metal ions. Each linear plot has the same slope, which is 0.50, consistently with the slope expected from Equation (20).

Conclusion

Metal ions have been shown to alter the driving force of electron transfer in ZnP–NIm through the strong binding of the metal ion with $NIm^{\bullet -}$. The rate constants of the photoinduced electron transfer from ^{1}ZnP* to NIm (CS process) are not affected by the change in the driving force in the presence of metal ions, since the CS process precedes the binding of metal ions with $NIm^{\bullet -}$. The k_{CS} values in the absence and in the presence of metal ions, as well as the k_{CR} values in the absence of metal ions, are well fitted to the Marcus equation for non-adiabatic electron transfer with the same λ and V values. The k'_{CR} values of back electron transfer in the $ZnP^{\bullet +}$–$NIm^{\bullet -}/M^{n+}$ complexes (CR process) in the presence of metal ions become much smaller than those in the absence of metal ions. The drastic change in the driving force of back electron transfer is accompanied by a large reorganization energy required for the electron transfer involving the metal ion complex. The driving force dependence of k'_{CR} of the $ZnP^{\bullet +}$–$NIm^{\bullet -}/M^{n+}$ complexes can also be evaluated well in the context of the Marcus theory of electron transfer in which both the driving force and the reorganization energy decrease with increasing concentrations of metal ions. This study therefore provides a new strategy for controlling the back electron-transfer processes of the charge-separated states by complexation with metal ions.

Experimental Section

Materials: All solvents and chemicals were of reagent grade quality, obtained commercially, and used without further purification unless otherwise noted. Scandium triflate [$Sc(OTf)_3$ (99%, F.W. = 492.16)] was purchased from Pacific Metals Co., Ltd. (Taiheiyo Kinzoku). Lutetium triflate [$Lu(OTf)_3$] was prepared as reported previously[24,39] and dried under vacuum evacuation at 403 K for 40 h prior to use. 1-Benzyl-1,4-dihydronicotinamide dimer [$(BNA)_2$] was prepared according to the literature.[32c,40] The synthesis of *N*,*N*′-dihexyl-1,4,5,8-naphthalene-tetracarboxylic 1,8:4,5-diimide (NIm-ref) was reported previously.[41] 5,10,15,20-Tetrakis-*p*-tolyl-21*H*,23*H*-porphine was purchased from Aldrich Co., USA. The tetramethyl-1,4-benzoquinone was purchased from Tokyo Kasei Organic Chemicals, Japan, and purified by recrystallization from ethanol.[42] Benzonitrile (PhCN) was purchased from Tokyo Kasei Organic Chemicals and distilled over P_2O_5 prior to use.[42]

Synthesis and characterization: Details on the synthesis and characterization of the compounds [ZnP–NIm (**1**), ZnP–Im–NIm (**2**), and ZnP–NIm–R• (**1R**•)] are reported elsewhere.[27] ZnP-ref (zinc 5,10,15,20-tetrakis-*p*-tolyl-21*H*,23*H*-porphinate) was prepared by addition of zinc acetate to 5,10,15,20-tetrakis-*p*-tolyl-21*H*,23*H*-porphine, followed by heating at reflux for 1 h in MeOH/MeCN.

Laser flash photolysis and fluorescence decay: Time-resolved fluorescence spectra were measured on a Photon Technology International GL-3300 instrument with a Photon Technology International GL-302, nitrogen laser/pumped dye laser system, equipped with a four-channel digital delay/pulse generator (Stanford Research System Inc. DG535) and a motor driver (Photon Technology International MD-5020). Excitation wavelength was 431 nm with use of POPOP (1,4-bis(5-phenyl-2-oxazolyl)benzene) (Wako Pure Chemical Ind. Ltd., Japan) as a dye. Fluorescence lifetimes were determined by an exponential curve fit with the aid of a microcomputer. Nanosecond transient absorption measurements were carried out with a Nd:YAG laser (Solar, TII) at 431 nm with the power of 20 mJ as an excitation source. The transient spectra were recorded on fresh solutions in each laser excitation. The experiments at various temperatures were carried out in a Unisoku thermostated cell

holder designed for low-temperature measurements. The time-resolved absorption spectra of NIm-ref (1×10^{-4} M) with 2.0×10^{-2} M Sc^{3+} in the presence of an excess amount of $(BNA)_2$ in PhCN were measured upon excitation at 355 nm with the power of 25 mJ. The solution was deoxygenated by argon purging for 10 min prior to the measurements.

Spectral measurements: The UV/Vis spectrum of ZnP–$NIm^{\bullet-}$ was recorded on a Hewlett Packard 8453 diode array spectrophotometer in a quartz cuvette (pathlength = 10 mm) at 298 K. A benzonitrile solution of ZnP–$NIm^{\bullet-}$ was prepared by the one-electron reduction of ZnP–NIm (1×10^{-5} M) with tetramethylsemiquinone radical anion, which was produced through the proportionation reaction between tetramethylhydroquinone and tetramethyl-1,4-benzoquinone in the presence of tetrabutylammonium hydroxide (TBAOH).[43]

Cyclic voltammetry: Cyclic voltammetry measurements were performed at 298 K on a BAS 100W electrochemical analyzer in deaerated PhCN containing 0.1 M Bu_4NPF_6 ($TBAPF_6$) as supporting electrolyte. A conventional three-electrode cell was used, with a platinum working electrode (surface area of 0.3 mm^2) and a platinum wire as the counter-electrode. The Pt working electrode (BAS) was routinely polished with a BAS polishing alumina suspension and rinsed with acetone before use. The measured potentials were recorded with respect to the $Ag/AgNO_3$ (0.01 M) reference electrode. All potentials (against Ag/Ag^+) were converted to values against SCE by adding 0.29 V.[44] All electrochemical measurements were carried out under an atmospheric pressure of argon with the same scan rate (0.1 $V s^{-1}$).

Acknowlegements

This work was partially supported by Grants-in-Aid (Nos. 13440216, 13555247, 11228205) and the Development of Innovative Technology (No. 12310) from the Ministry of Education, Culture, Sports, Science, and Technology, Japan, and for Scientific Research (21COE at Osaka University and Kyoto University Alliance for Chemistry). H. I. thanks the Nagase Foundation for financial support.

[1] a) *The Photosynthetic Reaction Center* (Eds.: J. Deisenhofer, J. R. Norris), Academic Press, San Diego, **1993**; b) *Anoxygenic Photosynthetic Bacteria* (Eds.: R. E. Blankenship, M. T. Madigan, C. E. Bauer), Kluwer Academic Publishing, Dordrecht, **1995**.

[2] a) R. A. Marcus, *Annu. Rev. Phys. Chem.* **1964**, *15*, 155–196; b) R. A. Marcus, *Angew. Chem.* **1993**, *105*, 1161–1171; *Angew. Chem. Int. Ed. Engl.* **1993**, *32*, 1111–1121; c) R. A. Marcus, N. Sutin, *Biochim. Biophys. Acta* **1985**, *811*, 265–322.

[3] For the Marcus inverted region, see: a) G. L. Closs, J. R. Miller, *Science* **1988**, *240*, 440–447; b) I. R. Gould, S. Farid, *Acc. Chem. Res.* **1996**, *29*, 522–528; c) G. McLendon, *Acc. Chem. Res.* **1988**, *21*, 160–167; d) J. R. Winkler, H. B. Gray, *Chem. Rev.* **1992**, *92*, 369–379; e) G. McLendon, R. Hake, *Chem. Rev.* **1992**, *92*, 481–490; f) N. Mataga, H. Miyasaka, *Adv. Chem. Phys.* **1999**, *107*, 431–496; g) S. Fukuzumi, Y. Yoshida, T. Urano, T. Suenobu, H. Imahori, *J. Am. Chem. Soc.* **2001**, *123*, 11331–11332.

[4] a) M. R. Wasielewski, *Photoinduced Electron Transfer* (Eds.: M. A. Fox, M. Chanon), Elsevier, Amsterdam, **1988**, Part A, pp. 161–206; b) M. R. Wasielewski, *Chem. Rev.* **1992**, *92*, 435–461; c) M. R. Wasielewski, G. P. Wiederrecht, W. A. Svec, M. P. Niemczyk, *Sol. Energy Mater. Sol. Cells* **1995**, *38*, 127–134.

[5] a) M. N. Paddon-Row, *Acc. Chem. Res.* **1994**, *27*, 18–25; b) K. D. Jordan, M. N. Paddon-Row, *Chem. Rev.* **1992**, *92*, 395–410.

[6] J. W. Verhoeven, *Adv. Chem. Phys.* **1999**, *106*, 603–644.

[7] a) A. Osuka, N. Mataga, T. Okada, *Pure Appl. Chem.* **1997**, *69*, 797–802; b) K. Maruyama, A. Osuka, N. Mataga, *Pure Appl. Chem.* **1994**, *66*, 867–872.

[8] a) D. Gust, T. A. Moore, A. L. Moore, *Acc. Chem. Res.* **1993**, *26*, 198–205; b) D. Gust, T. A. Moore, A. L. Moore, S.-J. Lee, E. Bittersmann, D. K. Luttrull, A. A. Rehms, J. M. DeGraziano, X. C. Ma, F. Gao, R. E. Belford, T. T. Trier, *Science* **1990**, *248*, 199–201; c) C. C. Moser, J. M. Keske, K. Warncke, R. S. Farid, P. L. Dutton, *Nature* **1992**, *355*, 796–802; d) C. C. Page, C. C. Moser, X. Chen, P. L. Dutton, *Nature* **1999**, *402*, 47–52.

[9] a) J. C. Chambron, S. Chardon-Noblat, A. Harriman, V. Heitz, J. P. Sauvage, *Pure Appl. Chem.* **1993**, *65*, 2343–2392; b) M.-J. Blanco, M. Consuelo Jiménez, J.-C. Chambron, V. Heitz, M. Linke, J.-P. Sauvage, *Chem. Soc. Rev.* **1999**, *28*, 293–305; c) J.-C. Chambron, J.-P. Collin, J.-O. Dalbavie, C. O. Dietrich-Buchecker, V. Heitz, F. Odobel, N. Solladie, J.-P. Sauvage, *Coord. Chem. Rev.* **1998**, *178–180*, 1299–1312; d) A. Harriman, J.-P. Sauvage, *Chem. Soc. Rev.* **1996**, *25*, 41–48.

[10] a) F. D. Lewis, X. Liu, J. Liu, S. E. Miller, R. T. Hayes, M. R. Wasielewski, *Nature* **2000**, *406*, 51–53; b) F. D. Lewis, R. L. Letsinger, M. R. Wasielewski, *Acc. Chem. Res.* **2001**. *34*, 159–170.

[11] a) V. Balzani, A. Juris, M. Venturi, S. Campagna, S. Serroni, *Chem. Rev.* **1996**, *96*, 759–834; b) M. R. Arkin, E. D. A. Stemp, R. E. Holmlin, J. K. Barton, A. Hormann, E. J. C. Olson, P. F. Barbara, *Science* **1996**, *273*, 475–480.

[12] a) H. Imahori, Y. Sakata, *Adv. Mater.* **1997**, *9*, 537–546; b) H. Imahori, Y. Sakata, *Eur. J. Org. Chem.* **1999**, 2445–2457; c) S. Fukuzumi, D. M. Guldi, *Electron Transfer in Chemistry Vol. 2* (Ed.: V. Balzani), Wiley-VCH, Weinheim, **2001**, pp. 270–337.

[13] a) H. Imahori, K. Hagiwara, M. Aoki, T. Akiyama, S. Taniguchi, T. Okada, M. Shirakawa, Y. Sakata, *J. Am. Chem. Soc.* **1996**, *118*, 11771–11782; b) C. Luo, D. M. Guldi, H. Imahori, K. Tamaki, Y. Sakata, *J. Am. Chem. Soc.* **2000**, *122*, 6535–6551; c) H. Imahori, K. Tamaki, D. M. Guldi, C. Luo, M. Fujitsuka, O. Ito, Y. Sakata, S. Fukuzumi, *J. Am. Chem. Soc.* **2001**, *123*, 2607–2617; d) S. Fukuzumi, K. Ohkubo, H. Imahori, J. Shao, Z. Ou, G. Zheng, Y. Chen, R. K. Pandey, M. Fujitsuka, O. Ito, O. K. M. Kadish, *J. Am. Chem. Soc.* **2001**, *123*, 10676–10683; e) H. Imahori, K. Tamaki, Y. Araki, Y. Sekiguchi, O. Ito, Y. Sakata, S. Fukuzumi, *J. Am. Chem. Soc.* **2002**, *124*, 5165–5174; f) T. Kesti, N. V. Tkachenko, V. Vehmanen, H. Yamada, H. Imahori, S. Fukuzumi, H. Lemmetyinen, *J. Am. Chem. Soc.* **2002**, *124*, 8067–8077.

[14] H. Imahori, D. M. Guldi, K. Tamaki, Y. Yoshida, C. Luo, Y. Sakata, S. Fukuzumi, *J. Am. Chem. Soc.* **2001**, *123*, 6617–6628.

[15] a) D. Gust, T. A. Moore, *The Porphyrin Handbook, Vol. 8* (Eds.: K. M. Kadish, K. M. Smith, R. Guilard), Academic Press, San Diego, CA, **2000**, pp. 153–190; b) D. Gust, T. A. Moore, A. L. Moore, *Res. Chem. Intermed.* **1997**, *23*, 621–651; c) D. Gust, T. A. Moore, A. L. Moore, *Acc. Chem. Res.* **2001**, *34*, 40–48.

[16] a) P. A. Liddell, D. Kuciauskas, J. P. Sumida, B. Nash, D. Nguyen, A. L. Moore, T. A. Moore, D. Gust, *J. Am. Chem. Soc.* **1997**, *119*, 1400–1405; b) D. Carbonera, M. Di Valentin, C. Corvaja, G. Agostini, G. Giacometti, P. A. Liddell, D. Kuciauskas, A. L. Moore, T. A. Moore, D. Gust, *J. Am. Chem. Soc.* **1998**, *120*, 4398–4405; c) D. Kuciauskas, P. A. Liddell, A. L. Moore, T. A. Moore, D. Gust, *J. Am. Chem. Soc.* **1998**, *120*, 10880–10886; d) D. Kuciauskas, P. A. Liddell, S. Lin, T. E. Johnson, S. J. Weghorn, J. S. Lindsey, A. L. Moore, T. A. Moore, D. Gust, *J. Am. Chem. Soc.* **1999**, *121*, 8604–8614.

[17] a) N. Martín, L. Sánchez, B. Illescas, I. Pérez, *Chem. Rev.* **1998**, *98*, 2527–2548; b) F. Diederich, M. Gómez-López, *Chem. Soc. Rev.* **1999**, *28*, 263–277.

[18] a) R. M. Williams, J. M. Zwier, J. W. Verhoeven, *J. Am. Chem. Soc.* **1995**, *117*, 4093–4099; b) R. M. Williams, M. Koeberg, J. M. Lawson, Y.-Z. An, Y. Rubin, M. N. Paddon-Row, J. W. Verhoeven, *J. Org. Chem.* **1996**, *61*, 5055–5062.

[19] a) P. S. Baran, R. R. Monaco, A. U. Khan, D. I. Schuster, S. R. Wilson, *J. Am. Chem. Soc.* **1997**, *119*, 8363–8364; b) D. I. Schuster, P. Cheng, S. R. Wilson, V. Prokhorenko, M. Katterle, A. R. Holzwarth, S. E. Braslavsky, G. Klihm, R. M. Williams, C. Luo, *J. Am. Chem. Soc.* **1999**, *121*, 11599–11600; c) J.-F. Nierengarten, C. Schall, J.-F. Nicoud, *Angew. Chem.* **1998**, *110*, 2037–2040; *Angew. Chem. Int. Ed.* **1998**, *37*, 1934–1936; d) A. W. Jensen, S. R. Wilson, D. I. Schuster, *Bioorg. Med. Chem.* **1996**, *4*, 767–779; e) J.-F. Eckert, J.-F. Nicoud, J.-F. Nierengarten, S.-G. Liu, L. Echegoyen, F. Barigelletti, N. Armaroli, L. Ouali, V. Krasnikov, G. Hadziioannou, *J. Am. Chem. Soc.* **2000**, *122*, 7467–7479.

[20] a) F.-P. Montforts, O. Kutzki, *Angew. Chem.* **2000**, *112*, 612–614; *Angew. Chem. Int. Ed.* **2000**, *39*, 599–601; b) D. M. Guldi, M. Maggini, G. Scorrano, M. Prato, *J. Am. Chem. Soc.* **1997**, *119*, 974–980; c) A. Polese, S. Mondini, A. Bianco, C. Toniolo, G. Scorrano, D. M.

Guldi, M. Maggini, *J. Am. Chem. Soc.* **1999**, *121*, 3446 – 3452; d) C. Luo, D. M. Guldi, M. Maggini, E. Menna, S. Mondini, N. A. Kotov, M. Prato, *Angew. Chem.* **2000**, *112*, 4052 – 4056; *Angew. Chem. Int. Ed.* **2000**, *39*, 3905 – 3909; e) D. M. Guldi, M. Prato, *Acc. Chem. Res.* **2000**, *33*, 695 – 703.

[21] a) S. Fukuzumi in *Electron Transfer in Chemistry, Vol. 4* (Ed.: V. Balzani), Wiley-VCH, Weinheim, **2001**, pp. 3 – 67; b) S. Fukuzumi, *Org. Biomol. Chem.* **2003**, *1*, 609 – 620; c) S. Fukuzumi, S. Itoh, *Adv. Photochem.* **1998**, *25*, 107 – 172.

[22] a) S. Fukuzumi, S. Koumitsu, K. Hironaka, T. Tanaka, *J. Am. Chem. Soc.* **1987**, *109*, 305 – 316; b) S. Fukuzumi, N. Nishizawa, T. Tanaka, *J. Chem. Soc. Perkin Trans. 2* **1985**, 371 – 378.

[23] a) S. Fukuzumi, T. Okamoto, J. Otera, *J. Am. Chem. Soc.* **1994**, *116*, 5503 – 5504; b) S. Fukuzumi, N. Satoh, T. Okamoto, K. Yasui, T. Suenobu, Y. Seko, M. Fujitsuka, O. Ito, *J. Am. Chem. Soc.* **2001**, *123*, 7756 – 7766; c) S. Fukuzumi, H. Mori, H. Imahori, T. Suenobu, Y. Araki, O. Ito, K. M. Kadish, *J. Am. Chem. Soc.* **2001**, *123*, 12458 – 12 465; d) S. Fukuzumi, Y. Fujii, T. Suenobu, *J. Am. Chem. Soc.* **2001**, *123*, 10191 – 10199.

[24] a) S. Fukuzumi, K. Ohkubo, T. Okamoto, *J. Am. Chem. Soc.* **2002**, *124*, 14147 – 14155; b) S. Fukuzumi, O. Inada, N. Satoh, T. Suenobu, H. Imahori, *J. Am. Chem. Soc.* **2002**, *124*, 9181 – 9188; c) S. Fukuzumi, J. Yuasa, T. Suenobu, *J. Am. Chem. Soc.* **2002**, *124*, 12566 – 12 573.

[25] a) S. Fukuzumi, K. Okamoto, H. Imahori, *Angew. Chem.* **2002**, *114*, 642 – 644; *Angew. Chem. Int. Ed.* **2002**, *41*, 620 – 622; b) S. Fukuzumi, K. Okamoto, Y. Yoshida, H. Imahori, Y. Araki, O. Ito, *J. Am. Chem. Soc.* **2003**, *125*, 1007 – 1013; c) K. Okamoto, H. Imahori, S. Fukuzumi *J. Am. Chem. Soc.* **2003**, *125*, 7014 – 7021.

[26] a) S. Fukuzumi, K. Ohkubo, *Chem. Eur. J.* **2000**, *6*, 4532 – 4535; b) S. Fukuzumi, K. Ohkubo, *J. Am. Chem. Soc.* **2002**, *124*, 10270 – 10271.

[27] Y. Mori, Y. Sakaguchi, H. Hayashi, *J. Phys. Chem. A.* **2002**, *106*, 4453 – 4467.

[28] For the radical anion of NIm, see: a) A. Osuka, S. Nakajima, K. Maruyama, N. Mataga, T. Asahi, I. Yamazaki, Y. Nishimura, T. Ohno, K. Nozaki, *J. Am. Chem. Soc.* **1993**, *115*, 4577 – 4587; b) A. Osuka, R. P. Zhang, K. Maruyama, T. Ohno, K. Nozaki, *Bull. Chem. Soc. Jpn.* **1993**, *66*, 3773 – 3782; c) A. Osuka, H. Shiratori, R. Yoneshima, T. Okada, S. Taniguchi, N. Mataga, *Chem. Lett.* **1995**, 913 – 914.

[29] The radical cation of Zn(TPP) (zinc 5,10,15,20-tetraphenyl-21*H*,23*H*-porphinate) has the characteristic broad absorption in 500 – 700 nm together with an intense band at 406 nm; see: J. Fajer, D. C. Borg, A. Forman, D. Dolphin, R. H. Felton, *J. Am. Chem. Soc.* **1970**, *92*, 3451 – 3459.

[30] The bleaching of the porphyrin Q band is observed at 560 nm in Figure 2a.

[31] In Figure 2b, only the absorption bands due to the $(NIm\text{-}ref)^{\bullet-}/Sc^{3+}$ complex are observed, since $(BNA)_2^{\bullet+}$ produced in the photoinduced electron transfer from $(BNA)_2$ to NIm-ref is converted into BNA^+, which has no absorption band in the visible region; see ref. [32].

[32] a) S. Fukuzumi, M. Patz, T. Suenobu, Y. Kuwahara, S. Itoh, *J. Am. Chem. Soc.* **1999**, *121*, 1605 – 1606; b) S. Fukuzumi, T. Suenobu, M. Patz, T. Hirasaka, S. Itoh, M. Fujitsuka, O. Ito, *J. Am. Chem. Soc.* **1998**, *120*, 8060 – 8068.

[33] The k_{CR} value is much smaller than that reported for a zinc porphyrin–naphthalenediimide dyad with a longer spacer (an additional phenyl group is inserted); see: H. Imahori, H. Yamada, D. M. Guldi, Y. Endo, A. Shimonura, S. Kundu, K. Yamada, T. Okada, *Angew. Chem.* **2002**, *114*, 2450 – 2453; *Angew. Chem. Int. Ed.* **2002**, *41*, 2344 – 2347. The k_{CR} value is hence highly sensitive to the spacer length of an electron donor–acceptor dyad.

[34] If the charge-separated state with a triplet spin multiplicity—$^3[ZnP^{\bullet+}\text{–}NIm^{\bullet-}]$—is formed, its decay rate could be determined by the spin conversion rate to give the singlet state $^1[ZnP^{\bullet+}\text{–}NIm^{\bullet-}]$(see ref. [27]). In such a case, the rate constant of the spin-allowed CR process, $^1[ZnP^{\bullet+}\text{–}NIm^{\bullet-}]\rightarrow$ZnP-NIm, would be larger than the observed decay rate constant. It should be noted, however, that the singlet excited state, ^{1}ZnP*, in ZnP-NIm undergoes the CS process with a high efficiency ($\Phi_{CS} = 0.89$), predominating over the intersystem crossing to give the triplet excited state ^{3}ZnP* ($\Phi_{ISC} = 0.09$).

[35] The transient absorption spectrum of **2** in the presence of Sc^{3+} also affords the absorption bands due to the $NIm^{\bullet-}/Sc^{3+}$ complex.

[36] The CS process of **2** may proceed in a stepwise manner. However, the absence of any intermediate in the fast spectroscopy indicates that the secondary charge-shift reaction would be much faster than the primary CS process (ref. [27]). The faster CS rate of **2** than of **1** (Table 1) may be attributed to this primary CS process.

[37] L. Meites, *Polarographic Techniques*, Wiley, New York, **1965**, 2nd ed., pp. 203 – 301.

[38] R. A. Marcus, *J. Phys. Chem. B* **1998**, *102*, 10071 – 10077.

[39] a) J. H. Forsberg, V. T. Spaziano, T. M. Balasubramanian, G. K. Liu, S. A. Kinsley, C. A. Duckworth, J. J. Poteruca, P. S. Brown, J. L. Miller, *J. Org. Chem.* **1987**, *52*, 1017 – 1021; b) S. Kobayashi, I. Hachiya, *J. Org. Chem.* **1994**, *59*, 3590 – 3596.

[40] K. Wallenfels, M. Gellrich, *Chem. Ber.* **1959**, *92*, 1406 – 1415.

[41] D. G. Hamilton, L. Prodi, N. Feeder, J. K. M. Sanders, *J. Chem. Soc. Perkin Trans. 1* **1999**, 1057 – 1066.

[42] D. D. Perrin, W. L. F. Armarego, D. R. Perrin, *Purification of Laboratory Chemicals 4th edition*, Pergamon Press, Elmsford, NY, **1996.**

[43] S. Fukuzumi, I. Nakanishi, T. Suenobu, K. M. Kadish, *J. Am. Chem. Soc.* **1999**, *121*, 3468 – 3474.

[44] C. K. Mann, K. K. Barnes, *Electrochemical Reactions in Nonaqueous Systems*, Marcel Dekker, New York, **1990**.

Received: June 17, 2003
Revised: September 23, 2003 [F5239]

